Valence and spin-state transition in cobaltates revisited by x-ray magnetic circular dichroism

F. Guillou,[1,*] K. Kummer,[1] Y. Bréard,[2] L. Hervé,[2] and V. Hardy[2]

[1]*ESRF, The European Synchrotron, 71 Av. des Martyrs, 38000 Grenoble, France*
[2]*CRISMAT Lab., UMR 6508 CNRS/ENSICAEN/UNICAEN, 6 Bd. Maréchal Juin, 14050 Caen, France*

The compounds $(Pr_{1-y}Sm_y)_{0.7}Ca_{0.3}CoO_3$ belong to a class of Pr-based cobaltates presenting a unique case of simultaneous valence (charge transfer between Pr and Co ions) and spin-state transition (of the Co^{3+} ions), hereafter referred to as VSST. The present study sheds light on the debated issues of the Co^{4+} and Co^{3+} spin states, by combining x-ray absorption spectroscopy (XAS) at Co and Pr edges and x-ray magnetic circular dichroism (XMCD) at Co $L_{2,3}$ edges. XAS experiments at both L_3 and $M_{4,5}$ Pr edges attest to the appearance of Pr^{4+} below the VSST at $T^* = 106$ K, and allow a precise characterization of the evolution of the Co^{4+} content as a function of the temperature. XMCD at the Co $L_{2,3}$ edges at 5 K, and in magnetic field up to 9 T, directly tackles the issue of the Co^{4+} spin state. It is found that the Co^{4+} ions are most likely in a low spin state, and experience ferromagnetic interactions at $T \ll T^*$. On the basis of temperature dependent XMCD at 9 T, the fingerprint of the VSST on the Co moments is isolated, and found to be consistent with bulk magnetization data when accounting for the rare-earth contributions derived from reference samples. These temperature dependent XMCD data are used to characterize the evolutions of the various valence/spin state of the Co species involved in the VSST. It appears that the Co^{3+} moments above T^* are not consistent with a pure intermediate spin state, whereas they can be well reproduced by considering a low/high spin mixture. Finally, these XMCD results are compared to those derived from fitting of the XAS spectra recorded in zero field at various temperatures.

I. INTRODUCTION

Spin-state transitions (SST) are among the most intriguing phenomena in solid state physics, and they have been the subject of continuing interest for more than 50 years. In transition-metal oxides, some cobaltates are known to possess this spin-state degree of freedom. In particular, the Co^{3+} cation located at an octahedral site can exhibit not only low-spin (LS) and high-spin (HS) states, but also an intermediate-spin state (IS) (formally noted $t_{2g}^5 e_g^1$ though it is expected to be a highly hybridized state). Since the 1950s, $LaCoO_3$ is the archetypical example of the studies on the SST related to Co^{3+} [1–4].

More recently, the observation of a first-order transition in some Pr-based cobalt oxides has opened new perspectives of research. In 2002, a metal-insulator transition accompanied by an abrupt drop in magnetization, a sharp peak in heat capacity, and a sudden decrease of the unit cell volume has been observed upon cooling at 90 K in $Pr_{0.5}Ca_{0.5}CoO_3$ [5]. Originally, this transition was interpreted as a first-order SST of the Co^{3+} from IS to LS upon cooling, while the Co^{4+} remained in an LS state at all temperatures. Subsequently, the same type of transition has been observed in various $(Pr,Ca,A)CoO_3$ materials with a partial substitution by $A = $ Y, Sm, Eu, Gd, Tb, and its interpretation has been revisited [6–10]. Indeed, it has been shown by analysis of neutron powder diffraction [11], low temperature heat capacity [12], and x-ray absorption spectroscopy (XAS) at the Pr L_3 edge [13] and Pr $M_{4,5}$ edges [14,15] that the Co spin-state transition is accompanied by a valence change of the Pr ions, from 3+ at room temperature towards $(3+\delta)+$ below the transition, with δ in the range 0.15–0.30 [12–18]. This appearance of Pr^{4+} at low temperatures is compensated by the Co ions, leading to a

decrease in Co^{4+} content below the transition, which occurs at a temperature hereafter denoted T*.

Despite a general agreement on the existence of a coupled valence and spin-state transition (VSST), many aspects of this transition are still ambiguous. In particular, conflicting pictures are found in the literature about the spin state of the Co ions. While it is well accepted that the Co^{3+} are in a low spin state at $T \ll T^*$, two major issues remain open. Which Co^{4+} spin state coexists with the Co^{3+} LS below the VSST? What is the nature of the Co^{3+} spin state above the VSST? About the first question, many reports pointed to a Co^{4+} LS state below the VSST, on the basis of magnetization, heat capacity, and XAS data [11–14,19]. Using the same techniques, however, the possibility of an intermediate spin state for Co^{4+} was also reported [15,20,21]. As for the Co^{3+} spin state above the VSST, one actually faces the longstanding controversy existing between a homogeneous IS state or a LS/HS mixture, in a way similar to that encountered in the case of $LaCoO_3$ [22]. Despite the use of various experimental techniques such as magnetic susceptibility [11,19–21], heat capacity [20], x-ray absorption and emission spectroscopies [13–15,23], or even high-field magnetization [24], there is still no consensus. It should be stressed that all these techniques provide only an indirect insight into the Co spin states. The interpretation of the bulk magnetization data, for instance, relies heavily on the subtraction of the rare-earth contribution(s), which is always delicate, in particular at low temperatures when the details of the crystal-field splitting become critical. In addition, no reference compound exists to evaluate indisputably the magnetic response of the quite unusual Pr^{4+} state. In other respects, quantitative determinations of the Co species from the decomposition of Co XAS spectra can also be problematic, as this approach relies on calculated or experimental references, which necessarily introduce some degrees of uncertainty.

*fguillou@ameslab.gov

The present study aims to get a direct insight into the field and temperature dependences of the Co magnetic moments by performing x-ray magnetic circular dichroism (XMCD) experiments at the Co $L_{2,3}$ edges. Such an element selective and orbital specific magnetization probe has the advantage to overcome the issues related to the rare-earth magnetic contributions when analyzing bulk magnetometry data. Moreover, since there is a general agreement that the Co^{3+} ions are in a nonmagnetic LS state at very low temperatures (below ≈ 10 K), XMCD experiments will reflect directly the magnetism of the Co^{4+} ions (thus its spin state), provided that the Co^{4+} content is otherwise determined. As the temperature is increased across the VSST, the spin state of the Co^{3+} is increased, but several schemes involving LS, IS, and HS can be invoked. The two most likely pictures in debate are (i) a homogeneous IS state and (ii) a mixed LS/HS state. Once again, XMCD experiments are in a position to distinguish them via the determination of the Co moments. For both the issues of the spin state of Co^{4+} (at $T < T^*$) and that of Co^{3+} (at $T > T^*$), an independent determination of the Co^{4+} content is crucial. To that end, the Pr valence needs to be determined by independent XAS experiments, so that the Co^{4+} content can be calculated through the charge balance. This essential preliminary step will be carried out at both praseodymium M and L edges. These two complementary XAS techniques (involving different orbitals, probing depths, and modes of analysis) allow one to get a robust determination of the Pr^{4+} content.

II. EXPERIMENTAL DETAILS

Polycrystalline samples of $(Pr_{1-y}Sm_y)_{0.7}Ca_{0.3}CoO_3$, with $y = 0$ and $y = 0.36$, were prepared by the same solid-state reaction method followed by high-pressure annealing, as that reported in [15]. The $y = 0.36$ material (presenting a VSST at about $T^* = 106$ K) is the object of the present study. The $y = 0$ sample is used as a reference of pure Pr^{3+} for XAS analysis, as this material is known not to present a VSST [8]. To get a reliable estimate of the rare-earth contributions to the magnetic data, experimental references were synthesized: $Pr_{0.7}Ca_{0.3}Ti_{0.3}Ga_{0.7}O_3$ provides direct access to the Pr^{3+} magnetism (nonmagnetic Ti^{4+} and Ga^{3+}), while $SmAlO_3$ is a reference for Sm^{3+} (nonmagnetic Al^{3+}). As for Pr^{4+}, we were unable to find an appropriate reference material, i.e., a compound in which this cation is the unique magnetic species, while being located at the cubo-octahedral sites of the perovskite structure. The reference materials were synthesized by direct solid state reaction, using adequate mixtures of Sm_2O_3, Al_2O_3 and Pr_6O_{11}, CaO, TiO_2, Ga_2O_3 powders. For $Pr_{0.7}Ca_{0.3}Ti_{0.3}Ga_{0.7}O_3$, the mixture was heated at $1200\,°C$ for 24 h in oxygen flux, then pressed in the form of bars which were sintered at $1200\,°C$ for another 24 h in oxygen flux. For $SmAlO_3$, the bars were sintered in air at $1300\,°C$ for 96 h. The magnetization measurements were carried out in a superconducting quantum interference device magnetometer (MPMS), or using the ACMS option of a physical properties measurement system (Quantum Design).

The x-ray absorption experiments at the Pr $L_{2,3}$ edges were carried out at the ID12 beamline of the European Synchrotron

Radiation Facility (ESRF) in a multipurpose end station [25]. The sample was mounted on a cold finger cryostat allowing the temperature of the sample to vary in the range 2.1–320 K. The HELIOS-II type undulator with a 52 mm period was used as insertion device. Fluorescence yield was collected simultaneously with two different detection schemes in backscattering geometry. A Si photodiode serves as a detection system for the total fluorescence yield (TFY). Due to a rather strong and temperature dependent scattering background, we also used an energy resolved detection scheme. The partial fluorescence was recorded by a silicon drift detector mounted at $20°$ with respect to the incident beam. The energy resolution allows the fluorescence signal of the Pr L fluorescence lines to be separated from the scattering background, as well as from the fluorescence of the other elements from the sample. The Pr L_3 spectra were recorded upon heating at 12 temperatures between 2.2 and 300 K.

XAS at the Co $L_{2,3}$ and Pr $M_{4,5}$ edges, as well as XMCD experiments at the Co $L_{2,3}$ edges, were carried out at the ID32 beamline, ESRF. The experimental end station allows one to reach magnetic fields up to 9 T and temperature on the sample down to 5 K [26]. A bulk polycrystalline sample ($2\times2\times5$ mm^3) was cleaved in an ultrahigh vacuum chamber (base pressure of the order of 10^{-9} mbar) before being transferred to the superconducting magnet. XAS were taken by moving continuously and synchronously the monochromator and the undulator gap. The total electron yield (TEY) detection method was used. The XAS spectra (in $B = 0$) for Co $L_{2,3}$ and Pr $M_{4,5}$ edges were recorded upon heating at 25 temperatures between 5 and 300 K. XMCD spectra at the Co $L_{2,3}$ edge were obtained as the difference between XAS spectra measured with opposite helicities in finite magnetic field. To ensure that the final XMCD spectra are free of experimental artifacts, the whole set of measurements is repeated for the opposite direction of the magnetic field. The XMCD data presented hereafter typically corresponds to the average of 32 XAS differences per magnetic field direction. Two sets of XMCD experiments were carried out at 5 K: a first series at 3, 5, and 9 T, and another one at nine magnetic fields up to 9 T. The XMCD experiments at 3, 5, and 9 T were repeated at six other temperatures up to 300 K. Note that the same piece of sample was used for the measurements in the soft and hard x-ray ranges.

XMCD allows for getting an experimental estimate of the magnetization in an element selective manner. The magneto-optical sum rules are commonly used to determine the orbital m_L and effective spin moments m_S^{eff}: $m_L = -(2qn_h)/(3r)$ and $m_S^{eff} = (-3p + 2q)n_h/r$, where p and q denote the integrals of the XMCD at the L_3 absorption edge and at both the L_3 and L_2 absorption edges, respectively; r represents the integrated area of the white lines of both L_2 and L_3 subtracted from a background modeled by step functions [27,28]. The number of holes in the 3d band (n_h) is determined from the Co^{3+}/Co^{4+} ratio, which is itself derived from the Pr valence by using usual ionic charge balance.

In the present case, the typical random error for the determination of the magnetic moment from XMCD can be estimated to be of the order of $\pm 5\%$. In addition two sources of systematic errors should be discussed. First, a magnetic
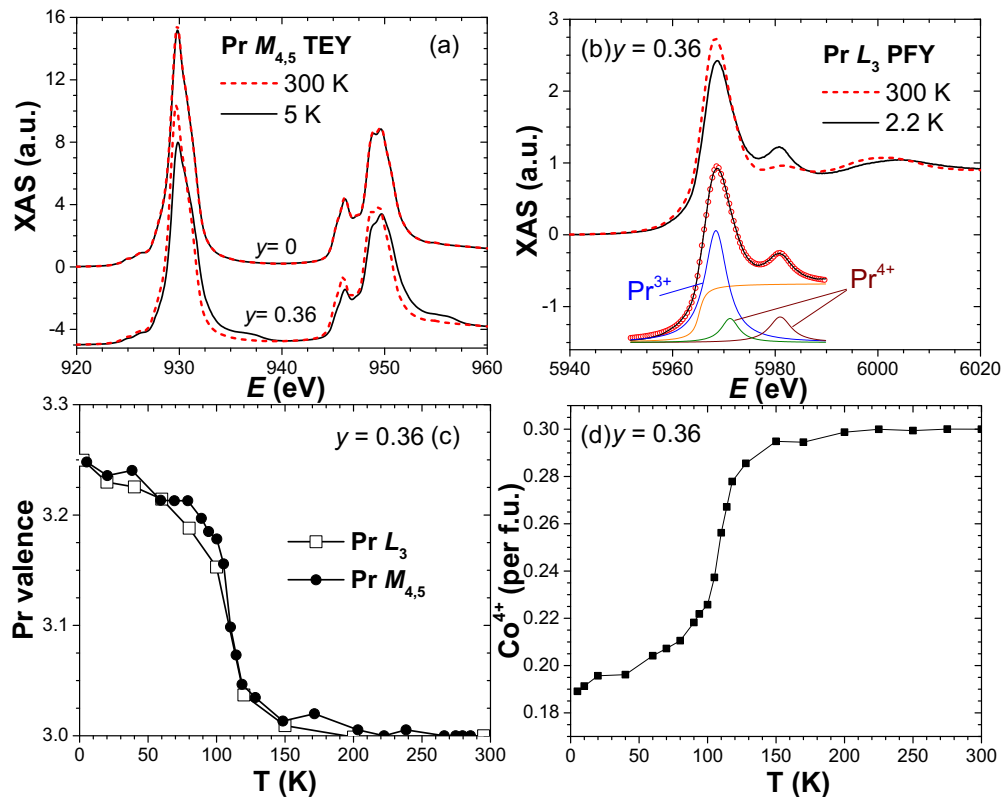
FIG. 1. (a) Pr spectra at the $M_{4,5}$ edges for $(Pr_{1-y}Sm_y)_{0.7}Ca_{0.3}CoO_3$ materials at two temperatures, for $y = 0$ and 0.36. (b) Pr spectra at the L_3 edge for $y = 0.36$, at room temperature (dashed curve) and at low temperature (solid curve). The lower set of curves illustrates the decomposition of the experimental spectrum at T = 2.2 K (solid curve), and its comparison to the reconstructed spectrum (open symbols). (c) Temperature dependence of the Pr valence derived from XAS measurements at L and M edges, for $y = 0.36$. (d) Temperature dependence of the Co^{4+} content inferred from the Pr valence, for $y = 0.36$.

dipole operator ($\langle T_Z \rangle$ term) has not been accounted for in our analysis. For a $3d$ transition metal, this term is usually considered to be very small with respect to the effective spin moment and is usually neglected [27]. For a $3d^5$ cation in an octahedral environment, a systematic evaluation of the $\langle T_Z \rangle$ term indeed indicates that the order of magnitude is about 10^{-3}–10^{-4}, irrespective of the temperature [29]. The second source of systematic error in the sum-rules analysis originates from the assumption that the absorption process does not involve a superimposition of $2p_{3/2}$ and $2p_{1/2}$ excitations. Experimental XMCD studies at the Co $L_{2,3}$ edges on closely related cobaltates either do not correct for orbital mixing as for LaCoO$_3$ [22] or consider only a limited correction factor 1.1 in (Pr,Sr)CoO$_3$ materials [30]. However, several theoretical works predict that the underestimation in the effective spin moment related to orbital mixing can be as high as $\sim$30% for a $3d^5$ ion [29,31]. At the end, our highest estimate of the relative error on the magnetic moments corresponds to the range -5% to $+23\%$.

III. RESULTS AND DISCUSSION

A. Determination of the Pr and Co valence as a function of the temperature

For the analysis of the XAS and XMCD data at the Co $L_{2,3}$ edges, in particular for a quantitative estimate of the Co

moments by the sum rules method, a crucial prerequisite is to determine independently the Co valence as a function of the temperature. This was herein inferred from the Pr^{4+}/Pr^{3+} ratio derived from analysis of the XAS spectra at the Pr M and L edges.

Figure 1(a) shows the Pr $M_{4,5}$ ($3d \rightarrow 4f$) XAS spectra for $y = 0$ and 0.36 at room temperature and at 5 K. For $y = 0$, there is no evolution of the spectrum, which remains typical of pure Pr^{3+} over the whole T range [32]. In contrast, a clear variation with T is observed for $y = 0.36$, revealing the development of Pr^{4+} at low temperatures. In this compound, XAS spectra at the Pr $M_{4,5}$ edges were recorded at various temperatures between 300 and 5 K. At each of them, the Pr valence was derived from a linear combination fitting of XAS spectra representative of Pr^{3+} ($y = 0$ material) and Pr^{4+}, as done in Ref. [15].

X-ray absorption experiments were also performed at the Pr L edge ($2p \rightarrow 5d$) as a function of the temperature. XAS spectra at the Pr L_3 edge for $y = 0.36$ are shown in Fig. 1(b) for T = 300 K and 2.2 K. The broadening of the main white line toward higher energies ($\sim$5 eV above the edge) and the development of an anomaly $\sim$12 eV above the main peak, which are visible at the lowest temperature, are typical of the development of Pr^{4+} [18]. The Pr L_3 spectra were analyzed in a way similar to that previously employed for this class of material [19]: first, the Pr^{3+} contribution is represented by a Lorentzian function accounting for most of

the white line, while the two additional Lorentzian functions at higher energies are attributed to Pr^{4+}; then, the Pr valence is determined from the ratio of their integrals, after a rescaling with respect to Pr^{3+} ($y = 0$ material) and $Pr^{3.67+}$ (Pr_6O_{11}) references.

The resulting estimates of the Pr valence from XAS at the $M_{4,5}$ and L_3 edges are shown in Fig. 1(c). One observes a sudden appearance of Pr^{4+} below the VSST, as systematically occurring in this type of transition [12–15]. The temperature resolution of the present study allows one to distinguish a certain dissymmetry in the valence change: the transition is quite sharp on its high temperature side, whereas Pr^{4+} continues to grow over a broad temperature range below T*. The good agreement between the results at the M and L edges deserves to be emphasized since these XAS experiments present several intrinsic differences. Beyond the fact that they probe different orbitals, in one case (M edge) the analysis relies on a spectral reconstruction based on linear combination fitting of experimental references, whereas in the other case (L edge), one uses a spectral decomposition into Lorentzian functions. Furthermore, given the large difference between the escape depth of the electrons during measurements at the Pr M edges (typically 1–5 nm) and the emitted fluorescence photons at the Pr L edges (of the order of 10 μm), the fair concordance between these experiments demonstrates that the VSST develops itself in a similar manner at the near surface and at much larger length scale. In the end, one can consider that the striking agreement observed in Fig. 1(c) between the two approaches brings support to the outcome of both analyses.

Using the average of the Pr^{4+} content derived from experiments at Pr M and L edges, the variation of the Co^{4+} content as a function of the temperature is calculated from the usual ionic balance (Sm^{3+}, Ca^{2+}, O^{2-}) [see Fig. 1(d)]. This determination of the Co valence forms the basis of the interpretation of XMCD data presented hereafter.

B. Field dependence of XMCD at low temperatures: Derivation of the Co^{4+} spin state

To tackle the issue of the Co^{4+} spin state below the VSST, XMCD experiments were carried out at our base temperature (T ≈ 5 K), as a function of the magnetic field up to the highest accessible value (9 T). In Fig. 2(a), the main panel shows raw XMCD data for selected magnetic fields, while the inset illustrates the background subtraction applied to the XAS spectra prior to integration for the XMCD sum rules. XMCD signals representing 0.5% to 3% of the XAS spectra are observed, which turn out to be one order of magnitude smaller than that of Co metal [28]. At 5 K (T ≪ T*), there is a general consensus on the fact that Co^{3+} ions are in a nonmagnetic low spin state. This implies that XMCD at Co $L_{2,3}$ edges only reflects the magnetization of the Co^{4+} ions, and thereby their spin state. At 5 K, the Co magnetic moments derived from the sum-rules analysis yield a ratio L/S of the orbital-to-spin components of about 0.4–0.45. This value is comparable to those typically found with Co^{3+} (0.2–0.5), while it is significantly lower than the one observed for Co^{2+} (0.57) [22,33]. In the absence of known correlation between L/S and the spin state in the case of Co^{4+}, we will limit ourselves herein to the study of the total magnetic moment.
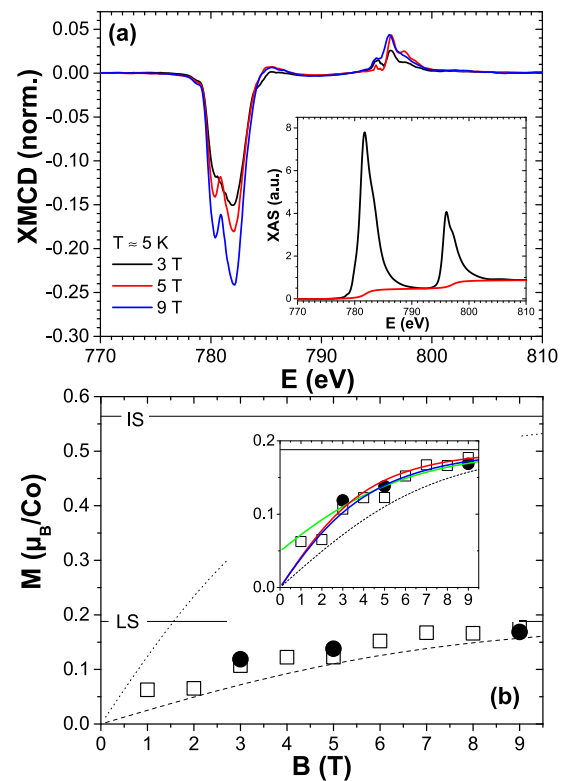
FIG. 2. (a) XMCD curves at the Co $L_{2,3}$ edges for $(Pr_{0.64}Sm_{0.36})_{0.7}Ca_{0.3}CoO_3$ at $T \approx 5$ K in different magnetic fields. The inset illustrates the background substraction for the sum-rules analysis on a corresponding XAS curve (average between two helicities for a given magnetic field). (b) Magnetic moments derived from XMCD experiments at 5 K by using the sum-rules analysis on two series of independent data (open squares and filled circles). The horizontal lines represent the expected saturation value for Co^{4+} LS ($S = 1/2$, $g = 2$) and for Co^{4+} IS ($S = 3/2$, $g = 2$). Magnetization curves calculated from a conventional Brillouin function are shown for Co^{4+} LS (dashed line) and Co^{4+} IS (dotted line). The inset is an enlargement showing various modelizations for the field dependence of the magnetization (see text): constant molecular field ($B_{mol} = 2$ T, green), Weiss molecular field [$\lambda = 15$ T/(μ_B/f.u.), blue], or clusterization ($p = 3$, red).

Two independent runs of measurements were performed, with different field increments [Fig. 2(b)]. In the low field range, the Co magnetic moment clearly increases with the magnetic field, before showing a tendency towards saturation at ∼0.18 μ_B/Co when approaching 9 T. Using the Co^{4+}/Co content (∼0.188) derived from Sec. III A, saturation magnetizations ($M_{sat} = gS\mu_B$) of about 0.188 μ_B and 0.564 μ_B can be anticipated for Co^{4+} LS ($S = 1/2$) and Co^{4+} IS ($S = 3/2$), respectively, when using a Landé factor $g = 2$. Clearly, it appears that the Co magnetization from XMCD is hardly compatible with a Co^{4+} IS state, while it is in fair agreement with a Co^{4+} LS state. Even if considering the highest estimate of the experimental uncertainty associated to the sum-rules analysis (+23%), the largest corrected cobalt magnetization (0.18×1.23 ≈ 0.22 μ_B) remains far from the expectation for Co^{4+} IS (0.188×2×3/2 ≈ 0.56 μ_B).

Since there is no long-range magnetic ordering below the VSST, the field dependence of the magnetization at

5 K is expected to follow a Brillouin function, at a first approximation. The magnetizations derived from this function for both Co^{4+} LS and Co^{4+} IS (Fig. 2) confirm the better reliability of the former spin state. In other respects, it is patent that the experimental data saturate faster than expected for a conventional Brillouin function (pure paramagnet). In materials presenting a VSST, such a deviation from standard paramagnetism at low temperature has been previously reported, and it is generally attributed to the presence of ferromagnetic interactions [12,19]. Such a feature can be taken into account in different ways. First, the field dependence of the Co magnetization (inset of Fig. 2) can be reproduced by considering a constant molecular field ($B_{eff} = B + B_{mol}$) in the Brillouin function, as formerly suggested to account for the Schottky anomaly related to Pr^{4+} in $(Pr,Y)_{0.7}Ca_{0.3}CoO_3$ materials [12,19]. Still within a mean-field approach, the enhanced trend to saturation of the Co magnetization at 5 K can also be attributed to a Weiss molecular field ($B_{eff} = B + \lambda M$). In other respects, the observed field dependence of the magnetization can alternatively be regarded as the response of an inhomogeneous magnetic state containing ferromagnetic Co^{4+} clusters [34,35]. In a rough approximation, this amounts to considering that N Co^{4+} ions of spin S ($=1/2$) should be replaced by N/p clusters of spin pS. As shown in the inset of Fig. 2, all these approaches result in acceptable overlaps between the XMCD data and the calculated field dependence of the magnetization for a Co^{4+} low spin state.

C. Co magnetic moment determined from XMCD as a function of the temperature: Derivation of the Co^{3+} spin state

Figure 3 shows the temperature dependence of the XMCD curves at the Co $L_{2,3}$ edges for our highest magnetic field of 9 T (top panel), as well as the corresponding magnetic moment (bottom panel). Regarding the overall amplitude of the XMCD signal, one clearly notices an unusual evolution upon heating: first, a swift decrease from 5 to 90 K, then a sudden increase between 90 and 120 K, and finally above 120 K the XMCD decreases again but more slowly. Looking in more details, one observes modifications in the spectral shape itself as the temperature is increased, which can be ascribed to changes in the populations of various Co species. In absence of undisputed XMCD experimental reference spectra for the different Co^{3+} and Co^{4+} possibly at play, we will limit ourselves to an approach in terms of sum-rules integration in order to get a quantitative estimate of the global magnetic moment. In terms of magnetization, the temperature evolution of the XMCD corresponds upon heating to a sharp jump in the Co magnetization at ~110 K. The impact on magnetization of the discontinuous change in Co spin state at the VSST is directly observed. Not only is there a very good agreement with the VSST temperature (T* ≈ 106 K), but the overall shape of the bulk magnetization as a function of the temperature is reproduced. To go further, let us consider the rare-earth magnetic contributions that can be derived from our reference materials. This is limited hereafter to the range T>T*, owing to the absence of a reliable reference compound for Pr^{4+}. The Pr^{3+} and Sm^{3+} contributions in $(Pr_{0.64}Sm_{0.36})_{0.7}Ca_{0.3}CoO_3$ were estimated using bulk magnetization measurements on
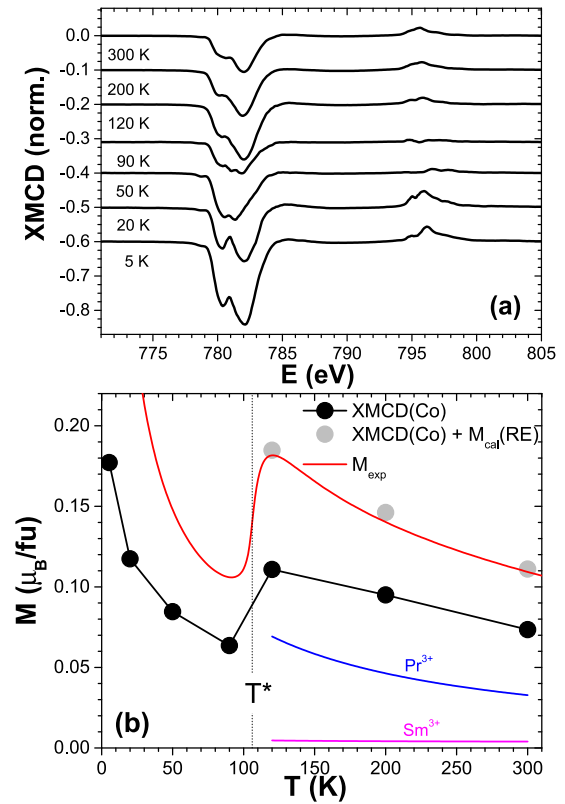
FIG. 3. (a) Co $L_{2,3}$ XMCD curves at different temperatures measured in $(Pr_{0.64}Sm_{0.36})_{0.7}Ca_{0.3}CoO_3$ at $B = 9$ T (an offset of 0.1 is used for clarity between the different temperatures). (b) Temperature dependence of the Co magnetic moment derived from XMCD through sum-rules analysis at $B = 9$ T (black circles), bulk magnetization of $(Pr_{0.64}Sm_{0.36})_{0.7}Ca_{0.3}CoO_3$ (red line), and combination of the XMCD data plus rare-earth contributions (gray circles). The blue (magenta) line is the calculated contribution of Pr^{3+} (Sm^{3+}) derived from the magnetization of $Pr_{0.7}Ca_{0.3}Ti_{0.3}Ga_{0.7}O_3$ (SmAlO$_3$).

$Pr_{0.7}Ca_{0.3}Ti_{0.3}Ga_{0.7}O_3$ and SmAlO$_3$, which are then converted to reflect 0.448 Pr^{3+} and 0.252 Sm^{3+} per formula unit. By combining these rare-earth contributions with the Co magnetization determined from XMCD, one obtains results in striking agreement with the bulk magnetization of $(Pr_{0.64}Sm_{0.36})_{0.7}Ca_{0.3}CoO_3$ [see Fig. 3(b)]. This supports the relevancy of the XMCD experiments at Co $L_{2,3}$ edge to isolate the Co magnetization, and thereby provides us with another means to address the issue of the Co^{3+} spin state, as detailed below.

In Fig. 3, the jump in the XMCD Co magnetization upon warming across T* is the combination of two processes: (i) an increase in the content of Co^{4+} due to the valence part of the transition and (ii) an increase in the average spin state of Co^{3+}, reflecting the spin-state part of the VSST. This latter mechanism involves a transformation from nonmagnetic Co^{3+} LS ($S = 0$) towards magnetic states of Co^{3+}, i.e., either Co^{3+} IS ($S = 1$) or Co^{3+} HS ($S = 2$). Since all the parameters of process (i) have been derived in previous sections (the spin state of Co^{4+} and the variation in temperature of its content), the XMCD data offers the possibility to shed light on the tricky question of the Co^{3+} spin state above the VSST. Let
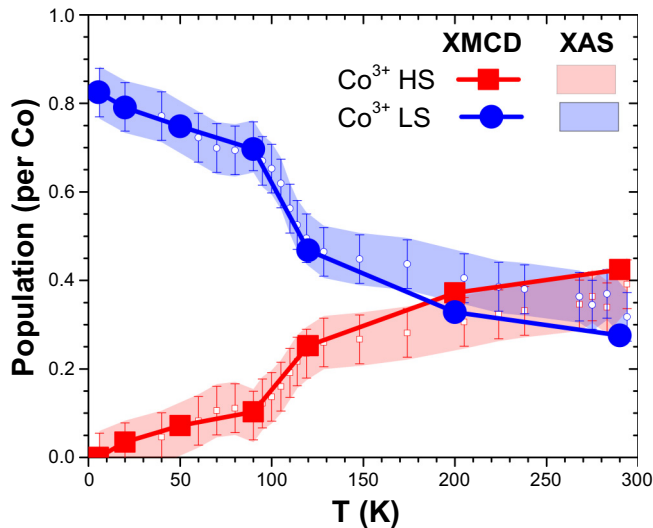
FIG. 4. Temperature dependence of the Co^{3+} HS (red squares) and Co^{3+} LS (blue circles) fractions derived from XMCD. The open symbols with shaded stripes correspond to the same fractions (red for Co^{3+} HS and blue for Co^{3+} LS) derived from XAS, including an estimate of the uncertainty ($+/-5\%$) associated to the fitting of the spectra.

us recall that the main controversy in the literature is between a homogeneous Co^{3+} IS state and an inhomogeneous Co^{3+} LS/HS state. Note also that we discard in the approach described below the possibility of tripartite mixtures (LS/IS/HS) for Co^{3+}, as well as any spin-state transition (towards IS or HS) for Co^{4+}. Accordingly, the average Co magnetization derived from XMCD can be simply written as the sum of two terms: $M_{\mathrm{XMCD}} = x_{Co^{4+}LS}(T) \times M_{Co^{4+}LS} + x'_{Co^{3+}}(T) \times M_{Co^{3+}}$. $x_{Co^{4+}LS}$ and $x'_{Co^{3+}}$ refer to the content (per Co) of Co^{4+} LS and of the "magnetic" Co^{3+} (i.e., either IS or HS). The values $M_{Co^{4+}LS}$, $M_{Co^{3+}IS}$, and $M_{Co^{3+}HS}$ are calculated from the Brillouin function, in a magnetic field of 9 T, by considering $g = 2$, as well as $S = 1/2$, $S = 1$, and $S = 2$ for Co^{4+} LS, Co^{3+} IS, and Co^{3+} HS, respectively. Using $x_{Co^{4+}LS}(T)$ shown in Fig. 1(d), the only left unknown is $x'_{Co^{3+}}(T)$, a quantity that can be calculated from M_{XMCD} considering either Co^{3+} IS or Co^{3+} HS. Then, $x_{Co^{3+}LS}(T)$ is obtained from the relationship $x_{Co^{4+}LS}(T) + x_{Co^{3+}LS}(T) + x'_{Co^{3+}}(T) = 1$.

First of all, it is found that the hypothesis of a pure IS state for the magnetic Co^{3+} is inconsistent with the XMCD data analyzed within the above approach. It even appears that a mixture LS/IS can be ruled out, since the XMCD data at the highest temperatures would lead to unphysical $x'_{Co^{3+}}(T)$ exceeding 1. In contrast, it turns out that reliable results can be obtained within the framework of a Co^{3+} LS/HS mixture. The temperature dependence of the Co^{3+} HS and LS fractions determined by this XMCD-based approach is displayed in Fig. 4. As the temperature is increased, one observes a smooth increase of the Co^{3+} HS fraction, with an acceleration at the VSST. It deserves to be noted that the Co^{3+} HS fraction starts growing at quite low temperatures (i.e., it is already noticeable at 20 K), and it continues to develop above T* up to our highest temperature of 300 K. This persistence of

a spin-state transformation above the VSST is in contrast with the evolution of the Co valence, which rather rapidly saturates above T*, as shown in Fig. 1(d). At room temperature, the XMCD experiments lead to the following distribution of cobalt species: $\sim$0.3 Co^{4+} LS, $\sim$0.27 Co^{3+} LS, and $\sim$0.43 Co^{3+} HS.

D. Comparison of the XMCD results to the XAS analysis in zero field

In a previous investigation of a close composition, (Pr$_{0.7}$Sm$_{0.3}$)$_{0.7}$Ca$_{0.3}$CoO$_3$ ($y = 0.3$), which was based uniquely on the fitting of XAS data, we were led to propose an intermediate spin state for Co^{4+} [15]. This conclusion turns out to be at odds with the Co^{4+} LS state revealed by the present XMCD study ($y = 0.36$). We do think that this discrepancy is not a matter of y value, and that the result of XMCD (i.e., Co^{4+} LS) must be regarded as being the most reliable, since this experimental technique is more suited to address this particular issue. Actually this problem points out the intrinsic difficulty associated to the reconstruction of XAS spectra made of many contributions (at least three Co species are at play in the VSST compounds). The situation is further complexified in the present case by the low amount of Co^{4+}, as well as the moderate spectral difference expected between the LS and IS signatures [36]. On top of that, the reliability of the experimental reference spectrum for Co^{4+} IS (SrCoO$_3$) is made fragile by the known great sensitivity of this compound to oxygen stoichiometry.

On the basis of the above remarks, let us readdress the issue of the XAS Co $L_{2,3}$ spectral analysis by considering Co^{4+} LS instead of Co^{4+} IS. In principle, the XMCD experimental data could have been used to guide the choice in CTM parameters and optimize the fitting of the XAS spectra [37]. At T = 5 K where only the XMCD from Co^{4+} LS should be considered [Fig. 5(a)], experimental and simulated XMCD curves share some similarities; however, the width of the main $L3$ peak is underestimated by the CTM simulations when using CTM parameters already reported for closely related cobaltates. This situation actually recalls that observed in (Pr,Sr)CoO$_3$ materials [30]. Given that several phenomena might be involved, and that the number of parameters increases with the development of magnetic Co^{3+} when raising the temperature, XMCD spectral simulations were not pursued further. In our XAS analysis based on spectral decomposition, we used the calculated reference spectra of Co^{3+} LS and HS previously described in [15], while a Co^{4+} LS reference was simulated by charge transfer multiplet calculations [37]. It turns out that works dealing with Co^{4+} ions are scarcer than for those of Co^{3+}. Yet, multiplet calculations of experimental XAS spectra have been carried out in a few Co^{4+} oxides: SrCoO$_3$ [36,38], Na$_x$CoO$_2$ [39], (La,A)CoO$_3$ thin films [33], (Pr,Ca)CoO$_3$ [14], (Pr,Sm,Ca)CoO$_3$ [15], (Pr,Sr)CoO$_3$ [30,40], and the most commonly used Co^{4+} LS reference BaCoO$_3$ [39]. This allowed us to define average parameters for a typical Co^{4+} LS [41].

The isotropic Co $L_{2,3}$ XAS spectra for a few selected temperatures are shown in Fig. 5(b) and put in regards to the calculated reference spectra for Co^{4+} LS, Co^{3+} LS, and HS. As T is increased, the overall behavior is similar to that reported in
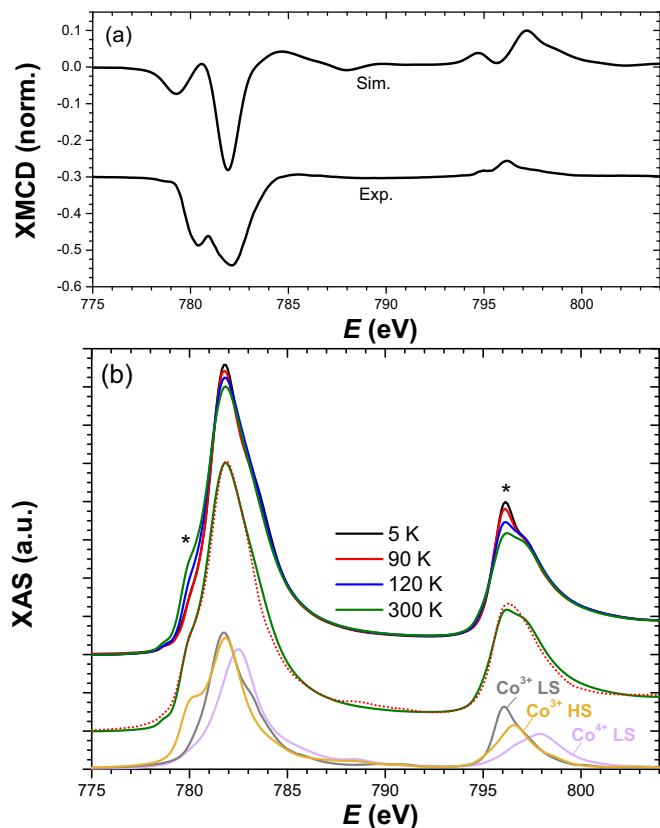
FIG. 5. (a) Comparison between experimental Co $L_{2,3}$ XMCD spectra at T = 5 K and B = 9 T, with simulated XMCD spectra by CTM for Co^{4+} LS. (b) Upper set of curves: experimental XAS spectra at selected temperatures (B = 0). The stars mark out the two features discussed in text. Intermediate set of curves: comparison between simulated (dotted line) and experimental (solid line) spectra at 300 K. Lower set of curves: calculated XAS reference spectra for Co^{4+} LS, Co^{3+} LS, and HS.

[15], the most noticeable evolutions being the appearance of a well distinguishable shoulder on the low energy side of L_3, and the disappearance of the peaky protuberance at the L_2 edge. These two distinguishable features are most often ascribed to the development of Co^{3+} HS at the expense of Co^{3+} LS, either in compounds presenting the VSST or in other cobaltates like $LaCoO_3$ [15,22]. In the determination of the Co populations from XAS spectra, the temperature dependence of these two features dominate the determination of the Co^{3+} LS/HS ratio. Given that the L_3 and L_2 white lines of Co^{4+} are located at significantly higher energies (see Fig. 5), it turns out that the nature of the Co^{4+} spin state only weakly interferes with the determination of the Co^{3+} LS/HS ratio in the XAS fitting process. For instance, the fitting of the XAS data at 300 K yields a Co^{3+} HS fraction that is ~0.38 when using Co^{4+} LS (with the present reference spectrum), while it would have been ~0.34 with Co^{4+} IS (as in [15]).

The Co populations for $(Pr_{0.64}Sm_{0.36})_{0.7}Ca_{0.3}CoO_3$ determined from the reconstruction of XAS spectra measured as a function of the temperature are presented in Fig. 4. One can note an overall agreement between the populations derived from XAS fitting and those obtained from the XMCD

analysis. The high temperature resolution of the present XAS data allows one to confirm previous remarks made in $(Pr_{0.7}Sm_{0.3})_{0.7}Ca_{0.3}CoO_3$ about the evolution of the Co^{3+} HS/LS ratio [15]. In particular, the Co^{3+} SST from LS to HS clearly appears as a gradual process spread over the whole temperature range, on top of which an acceleration takes place at the VSST. At room temperature, the Co^{3+} LS to HS transition is incomplete, leading to the following distribution of cobalt species: ~0.3 Co^{4+} LS, ~0.32 Co^{3+} LS, and ~0.38 Co^{3+} HS.

Although there is a good overall agreement between the XMCD and XAS results (see Fig. 4), a deviation emerges at the highest temperatures (e.g., 0.43 versus 0.38 for Co^{3+} HS at 300 K, respectively). In this regard, it must be kept in mind that both methods have their own limitations. For instance, the XAS analysis relies on a linear combination of reference spectra, whose accuracy can never be perfect. As for the XMCD analysis, let us emphasize that the spin-only approach adopted for the calculation of the individual magnetic moments is only an approximation. Taking all this into account, one can consider that the level of consistency observed between the XMCD and XAS results is quite satisfying.

IV. CONCLUSION

X-ray absorption (XAS) and magnetic circular dichroism (XMCD) experiments were carried out in the compound $(Pr_{0.64}Sm_{0.36})_{0.7}Ca_{0.3}CoO_3$, which presents a simultaneous valence and spin-state transition (VSST), centered at T*$\approx$106 K. The variation in temperature of the Pr valence was derived from XAS measurements, recorded both at the L_3 and at the $M_{4,5}$ edges. Combining the two sets of data yielded an accurate determination of the Pr^{4+} content, from which the evolution of the Co^{3+} and Co^{4+} contents versus temperature was derived.

We then performed XMCD experiments at Co $L_{2,3}$ edges, since they can provide a direct insight into the Co magnetization. Their analysis was limited to the sum-rules method allowing an experimental quantitative estimate of the magnetic moments. At 5 K, a saturation magnetization of ~0.18 μ_B/Co was evidenced from XMCD. In a simple ionic picture, and within the usual assumption of Co^{3+} being in a low spin state at very low temperatures, such a magnetization turns out to be well compatible with a Co^{4+} low spin state. Moreover, the shape of the field dependence of the XMCD data was found to be well reproduced by a Brillouin function including ferromagnetic interactions.

XMCD measurements versus temperature (in 9 T) were also used to address the question of the Co^{3+} excited state. The evolution of the average Co moment as the temperature is increased across T* was found incompatible with a homogeneous Co^{3+} intermediate state, whereas the XMCD data could be well accounted for by a Co^{3+} low-spin/high-spin mixing. Following another—and more frequent—approach, the XAS Co $L_{2,3}$ spectra (in zero field) were analyzed by combination fitting of calculated reference spectra. These data show a fair agreement with the XMCD results about the evolution of the Co^{3+} spin state over the whole temperature range.

Finally, we notice that this study well illustrates the complementarity between XAS and XCMD, in particular it

highlights the interest of XMCD to bring direct magnetic information when multiple species are at play, like in the present case of mixed valence Co^{3+}/Co^{4+} oxides showing a coupled valence and spin-state transition.

[1] J. B. Goodenough, J. Phys. Chem. Solids **6**, 287 (1958).

[2] P. M. Raccah and J. B. Goodenough, Phys. Rev. **155**, 932 (1967).

[3] V. G. Bhide, D. S. Rajoria, G. R. Rao, and C. N. R. Rao, Phys. Rev. B **6**, 1021 (1972).

[4] M. Abbate, J. C. Fuggle, A. Fujimori, L. H. Tjeng, C. T. Chen, R. Potze, G. A. Sawatzky, H. Eisaki, and S. Uchida, Phys. Rev. B **47**, 16124 (1993).

[5] S. Tsubouchi, T. Kyômen, M. Itoh, P. Ganguly, Y. Shimojo, Y. Morii, and Y. Ishii, Phys. Rev. B **66**, 052418 (2002).

[6] H. Masuda, T. Fujita, T. Miyashita, M. Soda, Y. Yasui, Y. Kobayashi, and M. Sato, J. Phys. Soc. Jpn. **72**, 873 (2003).

[7] T. Fujita, T. Miyashita, Y. Yasui, Y. Kobayashi, M. Sato, E. Nishibori, M. Sakata, Y. Shimojo, N. Igawa, Y. Ishii, K. Kakurai, T. Adachi, Y. Ohishi, and M. Takata, J. Phys. Soc. Jpn. **73**, 1987 (2004).

[8] T. Fujita, S. Kawabata, M. Sato, N. Kurita, M. Hedo, and Y. Uwatoko, J. Phys. Soc. Jpn. **74**, 2294 (2005).

[9] A. V. Kalinov, O. Y. Gorbenko, A. N. Taldenkov, J. Rohrkamp, O. Heyer, S. Jodlauk, N. A. Babushkina, L. M. Fisher, A. R. Kaul, A. A. Kamenev, T. G. Kuzmova, D. I. Khomskii, K. I. Kugel, and T. Lorenz, Phys. Rev. B **81**, 134427 (2010).

[10] T. Naito, H. Sasaki, and H. Fujishiro, J. Phys. Soc. Jpn. **79**, 034710 (2010).

[11] A. J. Barón-González, C. Frontera, J. L. García-Muñoz, J. Blasco, and C. Ritter, Phys. Rev. B **81**, 054427 (2010).

[12] J. Hejtmánek, E. Šantavá, K. Knížek, M. Maryško, Z. Jirák, T. Naito, H. Sasaki, and H. Fujishiro, Phys. Rev. B **82**, 165107 (2010).

[13] J. L. García-Muñoz, C. Frontera, A. J. Barón-González, S. Valencia, J. Blasco, R. Feyerherm, E. Dudzik, R. Abrudan, and F. Radu, Phys. Rev. B **84**, 045104 (2011).

[14] J. Herrero-Martín, J. L. García-Muñoz, K. Kvashnina, E. Gallo, G. Subías, J. A. Alonso, and A. J. Barón-González, Phys. Rev. B **86**, 125106 (2012).

[15] F. Guillou, Q. Zhang, Z. Hu, C. Y. Kuo, Y. Y. Chin, H. J. Lin, C. T. Chen, A. Tanaka, L. H. Tjeng, and V. Hardy, Phys. Rev. B **87**, 115114 (2013).

[16] H. Fujishiro, T. Naito, S. Ogawa, N. Yoshida, K. Nitta, J. Hejtmánek, K. Knížek, and Z. Jirák, J. Phys. Soc. Jpn. **81**, 064709 (2012).

[17] H. Fujishiro, T. Naito, D. Takeda, N. Yoshida, T. Watanabe, K. Nitta, J. Hejtmánek, K. Knížek, and Z. Jirák, Phys. Rev. B **87**, 155153 (2013).

[18] J. Herrero-Martín, J. L. García-Muñoz, S. Valencia, C. Frontera, J. Blasco, A. J. Barón-González, G. Subías, R. Abrudan, F. Radu, E. Dudzik, and R. Feyerherm, Phys. Rev. B **84**, 115131 (2011).

[19] J. Hejtmánek, Z. Jirák, O. Kaman, K. Knížek, E. Šantavá, K. Nitta, T. Naito, and H. Fujishiro, Eur. Phys. J. B **86**, 305 (2013).

[20] V. Hardy, F. Guillou, and Y. Bréard, J. Phys.: Condens. Matter **25**, 246003 (2013).

[21] F. Guillou, Y. Bréard, and V. Hardy, Solid State Sci. **24**, 120 (2013).

[22] M. W. Haverkort, Z. Hu, J. C. Cezar, T. Burnus, H. Hartmann, M. Reuther, C. Zobel, T. Lorenz, A. Tanaka, N. B. Brookes, H. H. Hsieh, H.-J. Lin, C. T. Chen, and L. H. Tjeng, Phys. Rev. Lett. **97**, 176405 (2006), and references therein.

[23] J. M. Chen, J. M. Lee, S. C. Haw, S. A. Chen, V. Hardy, F. Guillou, S. W. Chen, C. Y. Kuo, C. W. Pao, J. F. Lee, N. Hiraoka, H. Ishii, K. D. Tsuei, and Z. Hu, Phys. Rev. B **90**, 035107 (2014).

[24] A. Ikeda, S. Lee, T. T. Terashima, Y. H. Matsuda, M. Tokunaga, and T. Naito, Phys. Rev. B **94**, 115129 (2016).

[25] A. Rogalev and F. Wilhelm, Phys. Met. Metall. **116**, 1285 (2015).

[26] K. Kummer, A. Fondacaro, E. Jimenez, E. Velez-Fort, A. Amorese, M. Aspbury, F. Yakhou-Harris, P. van der Linden, and N. B. Brookes, J. Synchrotron Radiat. **23**, 464 (2016).

[27] P. Carra, B. T. Thole, M. Altarelli, and X. Wang, Phys. Rev. Lett. **70**, 694 (1993).

[28] C. T. Chen, Y. U. Idzerda, H.-J. Lin, N. V. Smith, G. Meigs, E. Chaban, G. H. Ho, E. Pellegrin, and F. Sette, Phys. Rev. Lett. **75**, 152 (1995).

[29] J. P. Crocombette, B. T. Thole, and F. Jollet, J. Phys.: Condens. Matter **8**, 4095 (1996).

[30] J. Padilla-Pantoja, J. Herrero-Martín, E. Pellegrin, P. Gargiani, S. M. Valvidares, A. Barla, and J. L. García-Muñoz, Phys. Rev. B **92**, 245136 (2015).

[31] C. Piamonteze, P. Miedema, and F. M. F. de Groot, Phys. Rev. B **80**, 184410 (2009).

[32] Z. Hu, G. Kaindl, H. Ogasawara, A. Kotani, and I. Felner, Chem. Phys. Lett. **325**, 241 (2000).

[33] M. Merz, P. Nagel, C. Pinta, A. Samartsev, H. v. Löhneysen, M. Wissinger, S. Uebe, A. Assmann, D. Fuchs, and S. Schuppler, Phys. Rev. B **82**, 174416 (2010).

[34] K. Knížek, J. Hejtmánek, M. Maryško, P. Novák, E. Šantavá, Z. Jirák, T. Naito, H. Fujishiro, and C. de la Cruz, Phys. Rev. B **88**, 224412 (2013).

[35] D. Phelan, K. P. Bhatti, M. Taylor, S. Wang, and C. Leighton, Phys. Rev. B **89**, 184427 (2014).

[36] R. H. Potze, G. A. Sawatzky, and M. Abbate, Phys. Rev. B **51**, 11501 (1995).

[37] E. Stavitski and F. M. F. de Groot, Micron **41**, 687 (2010).

[38] M. Abbate, G. Zampieri, J. Okamoto, A. Fujimori, S. Kawasaki, and M. Takano, Phys. Rev. B **65**, 165120 (2002).

[39] H.-J. Lin, Y. Y. Chin, Z. Hu, G. J. Shu, F. C. Chou, H. Ohta, K. Yoshimura, S. Hébert, A. Maignan, A. Tanaka, L. H. Tjeng, and C. T. Chen, Phys. Rev. B **81**, 115138 (2010).

[40] J. Padilla-Pantoja, J. Herrero-Martín, P. Gargiani, S. M. Valvidares, V. Cuartero, K. Kummer, O. Watson, N. B. Brookes, and J. L. García-Muñoz, Inorg. Chem. **53**, 8854 (2014).

[41] The typical parameters for the simulations of Co^{4+} ions by CTM are as follows: reduction of Slater integral to 80%–75% of their Hartree-Fock limit; $-1\,eV \leqslant \Delta \leqslant -3.5\,eV$ for Co^{4+} LS; $5.0\,eV \leqslant U_{dd} \leqslant 6.0\,eV$. The most crucial parameter turns out

to be related to the crystal-field splitting (10 Dq). In the study of $SrCoO_3$, combining experimental spectroscopy and atomic calculation including charge transfer, Potze *et al.* found the Co^{4+} high-spin state stable for 10 Dq < 0.6 eV, the intermediate spin state lays in the range 0.6 eV < 10 Dq < 1.1 eV, and the Co^{4+} low spin is obtained for 10 Dq > 1.1 eV [36]. The most frequent reported values for Co^{4+} LS are 2.0 eV < 10 Dq < 2.4 eV. A magnetic splitting parameter of 5 meV is considered.